Journal of African Earth Sciences 146 (2018) 15–27

Contents lists available at ScienceDirect

Journal of African Earth Sciences

journal homepage: www.elsevier.com/locate/jafrearsci

Neoproterozoic formation and evolution of Eastern Desert continental crust – The importance of the infrastructure-superstructure transition

Robert J. Stern

Geosciences Dept., U. Texas at Dallas, 800 W. Campbell Ave., Richardson, TX 75080, USA

ARTICLE INFO

Article history:
Received 18 October 2016
Received in revised form
22 December 2016
Accepted 2 January 2017
Available online 3 January 2017

Keywords:
Egypt
Neoproterozoic
Ophiolite

ABSTRACT

Neoproterozoic crust is beautifully exposed in the Eastern Desert (ED) of Egypt as an unbroken rift-flank uplift extending ~800 km between the Nile and the Red Sea, from near Cairo to the Sudan border. Different but related Neoproterozoic rocks are exposed in the northern, central and south Eastern Desert (NED, CED, and SED). Teleseismic data from four ED stations suggest that the crust is thin (28–33 km) and contains a mafic underplate ~5 km thick at its base. The CED is the best known of the three blocks because of low relief, good roads, and mineral deposits. The CED is mostly composed of Late Tonian-Cryogenian (~700–750 Ma) superstructure, of largely ensimatic character: disrupted ophiolitic crust with associated immature clastic sediments, diamictite, banded iron formation, and arc sequences. CED superstructure was deformed, metamorphosed to greenschist facies and especially ultramafic rocks pervasively altered by interaction with CO_2 –rich fluids of mostly mantle origin. Several domes bring deeper rocks of the gneissic infrastructure to the surface; these generally give younger radiometric ages than superstructure rocks, demonstrating that the infrastructure was hot, partially molten, and weak while the superstructure deformed above it. Special emphasis is given to a subhorizontal shear zone termed the Eastern Desert Decollement (EDD), localized at the boundary between brittle, greenschist-facies superstructure and ductile, partially molten infrastructure. The EDD was active during Najd strike-slip deformation ~600 Ma, but the infrastructure began forming in the south ~710 Ma, younging northward to the Ediacaran magmatic culmination in the NED. Melting of the infrastructure reflected magmatic underplating, now apparent as a 5 km –thick mafic lower crust. Fluid infiltration accompanying superstructure deformation and infrastructure magmatism were responsible for generating most of ED gold deposits. The SED is broadly similar to the CED but is poorly known. The NED is very different than the CED or SED and is almost entirely an Ediacaran magmatic construction, although minor relicts of Late Tonian –Cryogenian superstructure have been identified. Some suggestions for future studies are provided.

1. Introduction

We, like Prof. El Ramly, want to understand how the Neoproterozoic crust of the Eastern Desert of Egypt evolved and how this was accompanied by economically significant gold mineralization. Eastern Desert lithosphere is of interest to the global geoscience community because it is an excellent example of the ~4 million km^2 of Neoproterozoic lithosphere in N Africa (McKenzie et al., 2015). The hypotheses that we concoct for the formation of this lithosphere must be consistent with our overall understanding of the regional geology of this huge region, which at present is poor except for the Arabian-Nubian Shield (Johnson and Woldehaimanot, 2003). For better known regions such as the crust of Egypt, we must also explain the three-fold subdivision of the Eastern Desert (Stern and Hedge, 1985). The North, Central and South Eastern Desert domains (hereafter, NED, CED, and SED) all reveal different aspects of the region's protracted and intense Neoproterozoic episode of deformation and igneous activity. Surface exposures of the rocks of these three regions reveal different aspects of this evolution. In this contribution, I build on Prof. El Ramly's distinguished career of many years of research in the Eastern Desert to provide some new insights about how this crust evolved, and suggest some lines of future research. First, the subdivisions of the Eastern Desert are briefly reviewed. The Sinai peninsula also contains significant exposures of Neoproterozoic

E-mail address: rjstern@utdallas.edu.

http://dx.doi.org/10.1016/j.jafrearsci.2017.01.001
1464-343X/

crust but is not considered here because it is complicated by the presence of older ~1 Ga crust that is not recognized in the Eastern Desert (Be'eri-Shlevin et al., 2012; Abu El-Enen and Whitehouse, 2013); a review of Sinai Precambrian basement is needed. Along with outlining the most important features of the three Eastern Desert blocks, some ideas about ED crustal structure are presented. Specifically, the significance of the sharp transition from cool superstructure to hot infrastructure that existed ~600 Ma is emphasized. This transition separated partially molten felsic middle crust (infrastructure) from overlying greenschist-facies ensimatic assemblages (superstructure). This rheological boundary also localized Najd-related deformation and concentrated the fluids responsible for carbonate alteration of supracrustal ophiolitic peridotites, which in turn played an important role in generating gold-mineralized quartz veins. Below we briefly summarize the most important aspects of the three crustal domains, then explore how we can use this understanding to reconstruct processes happening ~600 Ma near this transition. In this review, I use internationally accepted subdivisions for Neoproterozoic time: Tonian (1000–720 Ma), Cryogenian (720–635 Ma), and Ediacaran (635–541 Ma). Fig. 1 uses this timescale to summarize the geologic history of the region, including many processes and relationships described in greater detail below.

2. Geologic overview

As noted above, the North, Central and South Eastern Desert domains (hereafter, NED, CED, and SED) all reveal different aspects of how the continental crust of the Eastern Desert formed. We start with the CED because it best preserves the oldest (Tonian-Cryogenian) history and also best preserves Ediacaran deformation as well as associated (Hammamat) basins, then the SED because it is just as old if not older than the CED, and finish with the NED, which is dominated by Ediacaran igneous rocks.

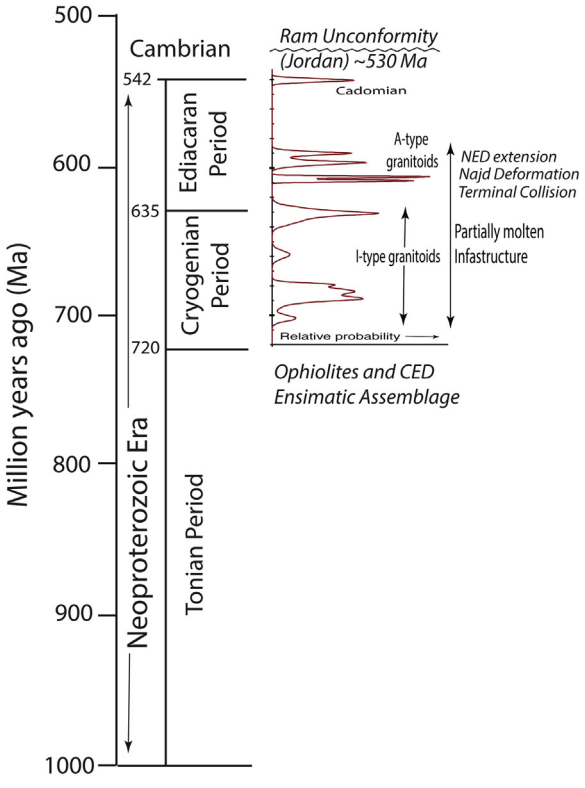

Fig. 1. Neoproterozoic time, showing time subdivisions used here. Also shown are the six Eastern Desert magmatic pulses identified by Augland et al. (2012) as well as the cutting of Rum unconformity as preserved in Jordan (Powell et al., 2014). This unconformity marks when the ANS – including the Eastern Desert - cooled completely and cratonized. "Cadomian" pulse ~540 Ma may be a far-field expression of Cadomian igneous activity as recently identified on the northern margin of the Arabian Plate (Stern et al., 2016).

2.1. The Central Eastern Desert

The CED is in many ways the best known of the three Eastern Desert subdivisions. This is partly due to its accessibility (it is traversed by two asphalt highways) and because it is a region of relatively subdued relief, but also because its supracrustal sequences are especially interesting and informative. The oldest evidence for how Eastern Desert crust formed is preserved in the Central Eastern Desert (CED), which is dominated by rocks of Cryogenian and Tonian age. The CED exposes an ensimatic (oceanic) assemblage characterized by a wide range of mostly greenschist-facies ophiolitic rocks and arc volcanics, along with volcaniclastic wackes, banded iron formation (BIF), and diamictite (Fig. 2B, C, D). The ensimatic assemblages represents the oldest documented CED units, with ~750 Ma U-Pb zircon ages (Kröner et al., 1992; Andresen et al., 2009; Ali et al., 2009). The supercrustal ensimatic assemblage is punctured by Cryogenian I-type granitoids and Ediacaran A-type granites (Fig. 1) and are further disrupted by several Ediacaran magmatic-metamorphic core complexes. These are locations where infracrustal "Tier 1" of Bennett and Mosely (1987) "poke through" lower-grade rocks of the superstructure ("Tier 2" of Bennett and Mosely, 1987). CED supracrustal sequences are locally overlain by Ediacaran (~600 Ma) successor basins of the Hammamat Group. Hammamt basins formed in response to differential relief between higher regions in the NED and lower regions in the CED that accompanied Najd deformation in the CED and magmatic rifting in the NED.

Eastern Desert infrastructure consists of upper amphibolite-facies quartzofeldspathic (granitic) gneisses and amphibolites exposed in several places in the CED, including the Meatiq, Abu Had, El Shalul, and El Sibai domes as well as the Migif-Hafafit and Beitan domes in the SED (Fig. 2B). These gneisses are intruded by dioritic, granodioritic, and granitic plutons, which likely formed in the infrastructure and differentially rose up through weak crustal shear zones. The contact between superstructure and infrastructure is sometimes an intrusive contact and sometimes a high-strain mylonitic zone. The infrastructure of the Eastern Desert is described in greater below in the section "Infrastructure" below.

The CED is perhaps best known for its abundance of ophiolitic rocks, which makes up the base of the superstructure. CED ophiolites are mostly highly disrupted and carbonated, although complete if abbreviated sequences of peridotites, gabbros, and pillow basalts can be found in a few places, for example along the Qena-Quseir road near Fawakhir and at Wadi Ghadir. Abdel-Karim and Ahmed (2010) summarized what is known about 38 different ophiolitic occurrences in the CED and SED. The volcanic section of these all show clear evidence of forming over a subduction zone, although it is controversial whether these formed in a backarc basin or in a forearc during subduction initiation (Abd El-Rahman et al., 2009a, b; Farahat, 2010).

Understanding the significance of Eastern Desert ophiolitic ultramafics is an especially difficult challenge because these are heavily altered by carbonate and disrupted by intense shearing. It is controversial how many episodes of deformation occurred but it is clear that ~600 Ma Najd deformation strongly affected the CED (Abdeen and Greiling, 2005). Serpentinized peridotites and related talc-carbonates are very weak and easy to deform so these tend to localize major faults and shear zones. As a result, they readily form

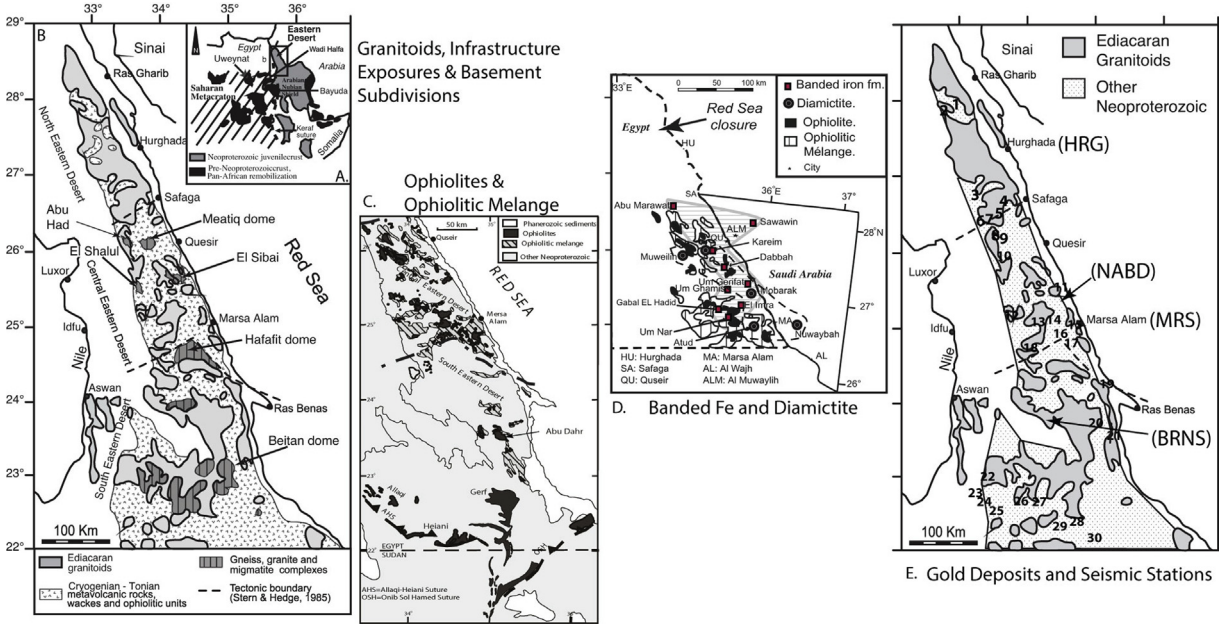

Fig. 2. (A) Reconstructed Arabian-Nubian Shield, showing location of the Eastern Desert as the NW flank of the Arabian-Nubian Shield. B) Geological map of the Eastern Desert of Egypt showing granitoids, gneisses, and arc units, along with basement subdivisions of North, Central, and South Eastern Dessert (modified after Ali et al., 2015). C): Map showing the distribution of ophiolites and ophiolitic mélanges in the Eastern Desert, modified after Shackleton (1994). D) The northern ANS banded iron formation (BIF) -ophiolite-diamictite basin, modified after Ali et al. (2010a,b). Map of pertinent regions of Egypt and Saudi Arabia with Red Sea closed, showing eight BIF localities in the Central Eastern Desert (CED) of Egypt (Sims and James, 1984) and Sawawin BIF in Arabia are shown with squares (Goldring, 1990). The association of BIF, diamictite and ophiolite is taken to outline a ~750 Ma marine basin. E) Locations of significant vein-type gold deposits (from Zoheir et al., 2008) and seismic stations (from Hosny and Nyblade, 2016) in the Eastern Desert of Egypt. Gold deposits: 1 = Um Mongul, 2 = Um Balad, 3 = Fatira, 4 = Abu Marawat, 5 = Semma, 6 = Hamana, 7 = Erediya, 8 = Atalla, 9 = Fawakhir, 10 = El Sid, 11 = Um Rus, 12 = Barramiya, 13 = Dungash, 14 = Atud, 15 = Sukkari, 16 = Hanglaliya, 17 = Um Ud, 18 = Hamash, 19 = Abu Rahaya, 20 = Um Eleiga, 21 = Hutit, 22 = Hariari, 23 = Haimur, 24 = Um Garaiart, 25 = Atshani, 26 = Murra, 27 = Seiga, 28 = Umm Tuyur, 29 = Betam, 30 = Um Egat. Seismic stations are at Hurghada (HRG), near Abu Dabbab (NABD), Marsa Alam (MRS) and Berenice (BRNS).

mélange (Fig. 2C) and are easily mylonitinized so that some altered peridotites are so intensely sheared as to appear in the field to be bedded metasediments. Fortunately, modern orbital remote sensing technology allows us to identify the distinct spectral characteristics from space (Sultan et al., 1986). It is clear that altered ultramafic rocks are especially abundant in the CED and also common in the SED (El Ramly, 1972). Studies of CED ophiolitic ultramafics show that, before serpentinization and carbonation, these were highly depleted harzburgites (Azer and Stern, 2007; Khalil and Azer, 2007); such depleted peridotites are only found in forearc environments today. Abd El-Rahman et al. (2012) proposed that CED ophiolitic sequences in the west formed in a forearc whereas those in the east formed in a backarc basin, but this interpretation is not yet convincing.

Sedimentary rocks are important supracrustal components of the CED above the ophiolites. These are thick sequences of greenschist-facies arc volcanics and associated wackes and volcaniclastics. Early ideas that CED arc volcanic sequences stratigraphically overlie ophiolites and metasediments (Stern, 1981) are not supported by U-Pb zircon geochronology. No discernible difference in age is found for ophiolites and arc sequences; both range in age from ~730 to ~750 Ma. One of the most interesting features of the arc metavolcanics is the abundance of pre-Neoproterozoic zircon xenocrysts in them (Stern et al., 2010). These volcanics show no isotopic evidence for involvement of pre-Neoproterozoic crust, leading Stern et al. (2010) to conclude that the old zircons were inherited from the mantle. No modern studies of CED metasediments have been carried out; we know these are related to the BIF and Atud diamictite and are broadly andesitic in bulk composition, but not much more.

The Atud diamictite is an especially interesting component of supracrustal metasediments. It is limited to the CED (although a correlative unit, the Nuwaybah diamictite, is identified in coastal Saudi Arabia (Ali et al., 2010a). Ali et al. (2010a) dated zircons from eight Atud diamictite clasts (five granitoids, 1 quartzite, 1 quartz porphyry, and 1 arkose) and a matrix sample from the diamictite. The clasts gave a mixture of ages. Two granitic clasts contained only Neoproterozoic (~750 Ma) zircons; another granitoid clast yielded mostly Neoproterozoic (750–790 Ma) along with abundant 2.1–2.4 Ga zircons; a fourth granitoid also yielded Paleoproterozoic (2006 ± 15 Ma) ages, which were partially reset in Neoproterozoic time; the fifth granitoid clast yielded only Paleoproterozoic–Archean ages. The quartz porphyry clast yielded mostly Neoproterozoic ages (697–778 Ma) along with one Early Paleoproterozoic and one Archean zircon. The quartzite clast yielded Paleoproterozoic to Archean (2093–2732 Ma) zircons. The arkose clast contained Neoproterozoic (722–773 Ma) and older Paleoproterozoic zircons (1.8–2.5 Ga). The diamictite matrix contains zircons that were derived from mixed Neoproterozoic and Paleoproterozoic sources (Ali et al., 2010a). As noted above, reliable pre-Neoproterozoic radiometric ages for in situ units in the CED or anywhere else in the Eastern Desert are unknown, so the pre-Neoproterozoic clasts and matrix in the Atud diamictite must have been derived from outside the CED and deposited in the oceanic basin that existed in the CED ~750 Ma. Ali et al. (2010a) suggested that this material may have been eroded by glacial activity during the Sturtian (~730 Ma) glacial episode from the Saharan Metacraton to the west (Abdelsalam et al., 2002), where pre-Neoproterozoic and Neoproterozoic crust are both abundant (Sultan et al., 1994).

Another diagnostic CED supracrustal unit is banded iron formation (BIF; El-Shazly and Khalil, 2014). BIFs occur at thirteen

localities scattered over ~30,000 km^2 in the CED (Fig. 2D). There is only one correlative BIF in Saudi Arabia, the Sawawin deposit (Stern et al., 2013). Where we can get age constraints, these BIFs seem to have formed ~750 Ma. The BIFs consist of interlayered dense magnetite and hematite layers alternating with jasper. BIFs and interbedded wackes are strongly deformed and metamorphosed to greenschist and occasionally amphibolite facies. They are clearly related to distal submarine igneous activity and may reflect re-oxygenation of the ocean associated with the Sturtian glaciation.

The important point is that ~750 Ma, what is today the CED was a crustal tract that had an oceanic crustal structure, with ~6 km thick oceanic crust associated with arc volcanics and overlain by sediments. It is not clear when and how this region attained its present thickness of ~30 km (Hosny and Nyblade, 2016). An important clue comes from the distribution of ~600 Ma Hammamat sediments, which define ~600 Ma basins and show that the much of the northern CED was low relative to the NED at this time (Fig. 2, Abdeen and Greiling, 2005), further suggesting that CED crust was relatively thin at that time. Hammamat basins are filled with coarse clastic sediment that was largely eroded from the NED and carried by one or more rivers south and deposited in terrestrial basins that are now best preserved in the northern CED, for example the Kareim Basin. The course of the Ediacaran river can be traced along the western flank of the Meatiq Dome (strongly deformed conglomerates of Wadi Um Esh; Ries et al., 1983) which opens up southward into a broad expanse of Hammamat NW of Wadis Hammamat, El Qash, and Arak (Fowler and Osman, 2013). Hammamat basins formed about the same time as Najd shearing, Dokhan Volcanism and intrusion of pink A-type granites, ~600 Ma.

We are beginning to understand the deformation history of the CED. Clearly Najd deformation during the interval 620–580 Ma strongly affected the region (Stern, 1985) but what was its deformation history before the Ediacaran collision, particularly that accompanying terrane accretion (e.g., Ries et al., 1983)? A clear story has yet to emerge. What is important for this study is that deformation of the superstructure was brittle, with abundant faults and shear zones, whereas deformation of the infrastructure was ductile and damage zones were often healed by magmas.

The northern limit of the CED is a diffuse boundary marked by intrusions of granitic batholiths of the southern part of the NED. This transition is marked by increased metamorphic grade northwards – from greenschist to amphibolite facies as the NED batholith is approached. It is more of a broad transition zone than a sharp boundary and lies south of the Qena-Safaga road. The NED-CED transition zone has not yet been studied in any detail but may mark where the infrastructure-superstructure boundary intersects the surface. Another window into the infrastructure-superstructure boundary is found south of the NED-CED boundary, around the Meatiq dome (Fig. 2B). There, the transition between infrastructure and superstructure is mostly structural (a shear zone), partly intrusive.

The southern limit of the CED is sharp, structural, and lies along the northern flank of the Migif-Hafafit dome (Fig. 2B; Shalaby, 2010). There are several explanations for the detailed structural history of the Migif-Hafafit complex, but for the purposes of this review, it represents an excellent window into the infrastructure-superstructure transition and the nature of the infrastructure. The boundary is a complex fault system that can be traced for several tens of kilometers NW along Wadi Nugrus and Gebel Hafafit, then turns abruptly SW along Gebel Migif and Wadi Shait to mark the boundary between superstructure and the CED to the north and infrastructure and the SED to the south.

2.2. The South Eastern Desert

The SED differs from the CED in several ways. First of all, it is much less studied, partly a reflection of its remote location and lack of asphalt roads. Second, it lacks interesting sediments such as BIF and diamictite. Third, it has some volcanogenic massive sulfide deposits whereas the CED does not (Abd El-Rahman et al., 2012). Fourth, it lacks significant Ediacaran sedimentary or volcanic successions such as the Hammamat Group and Dokhan Volcanics found in the NED and CED. The Shadli metavolcanics are superficially similar to the Dokhan but are significantly older (~710 Ma; Stern et al., 1991). The SED and CED contain similar proportions of serpentinites but these are scarcely studied except for ophiolites along the E-W trending Allaqi-Heiani-Gerf suture in the far south SED (Zimmer et al., 1995; Gahlan and Arai, 2009; Ali et al., 2010b; Azer et al., 2013; Abdel-Karim et al., in press) and at Abu Dahr (Gahlan et al., 2015) (Fig. 1C). In general there are few modern studies of SED basement. It seems to also show infrastructure-superstructure relationships like those of the CED, but the units in the SED are somewhat older. The SED in general seems to generally represent a deeper level of exposure than the CED and is less affected by Najd shearing. Because the SED is less studied than the CED, there is less geochronologic data here; what is available suggests that it is generally slightly older than the CED (Stern and Hedge, 1985), but more geochronological studies are needed.

2.3. The North Eastern Desert

The NED is very different than either the CED or the SED. Ophiolites are absent and gneisses are rare. BIF and Atud diamictite is unknown from the NED. Najd deformation is also missing. Instead, the NED is overwhelmingly composed of a wide range of Ediacaran igneous rocks and associated Hammamat sediments. There is strong evidence for extension, in the form of abundant ~600 Ma bimodal dike swarms that trend E-W to NE-SW, indicating ~ N-S oriented extension about the same time that Najd strike-slip deformation was affecting the CED (Stern et al., 1984). Abundant epizonal A-type granites also require passive emplacement and indirectly demonstrate strong extension. The Dokhan Volcanics were also thought to have erupted during this "magmatic flare-up" (Stern and Hedge, 1985; Wilde and Youssef, 2000). It was thought up to recently that the overwhelming majority of NE Desert igneous rocks and associated Hammamat sediments were ~600 Ma, but recent investigations show that it is not quite this simple. Breitkreuz et al. (2010) reported U–Pb zircon SHRIMP ages for 10 Dokhan silica-rich ignimbrites and two subvolcanic dacitic bodies from the NED. These ages range between 592 and 630 Ma, indicating that Dokhan volcanism occurred over a 40 Ma timespan.

The crustal subdivision of infrastructure and superstructure is not as useful for understanding the NED as it is for the CED and perhaps the SED. It is also noteworthy that Najd shears are not documented from the NED. There may have been some such relationship early in the evolution of the NED, but the Ediacaran magmatic flux overwhelmed the superstructure. There are hints that superstructure once existed in the NED. One of the most exciting recent developments in studies of the NED is that we are beginning to identify small tracts of pre-Ediacaran crust. We have known since Stern and Hedge (1985) that there are some older (Cryogenian and Tonian) igneous rocks, including the 666 Ma Mons Claudianus granodiorite, but new studies are discovering more and older crustal remnants. From a region SW of Gebel Dara near 27°50′ N where previous Rb-Sr geochronology suggest the presence of Tonian muscovite tonalite (Abdel-Rahman and Doig, 1987), Eliwa et al. (2014) documented the presence of I-type muscovite

trondhjemite and granodiorite with complex SIMS U-Pb zircon ages of ~740 Ma. Bühler et al. (2014) studied supracrustal units from this same region and documented the presence of ~720 Ma ignimbrites unconformably overlying the ~740 Ma granitoids, and Abd El-Rahman et al. (2017) documented that ~780 Ma dacite is also found in this small region. These ages are similar to those of CED crustal units, and these units may be related but further effort to identify and study slivers of Cryogenian-Tonian crust hidden in the NED will be need to evaluate this possibility.

3. Geophysical background

Geophysical data provides important constraints needed for understanding the crust of any region. A wide range of datasets are needed in order to understand crustal composition and structure at depth, including inferences from passive (teleseismic) networks, like Earthscope Transportable Array < http://www.usarray.org/researchers/obs/transportable>, active source (reflection and refraction seismology, like Lithoprobe; Hammer et al., 2010) seismic experiments, gravity and magnetics. Unfortunately, there are few such geophysical constraints for the Eastern Desert, with only passive seismic data providing broad constraints on crust and upper mantle structure. There are four seismic stations in the Eastern Desert; three are broadband stations (VBB) and one is a short-period station (SP): (Hurghada (HG; VBB); Abu Dabbab (NABD; SP), Marsa Alum (MRS; VBB), and Berenice (BRNS; VBB) (locations shown in Fig. 1E). Hosny and Nyblade (2016) performed receiver function analysis on teleseismic arrivals from these and other seismic stations in Egypt, but we are only interested in results for the 4 Eastern Desert stations here. These results are summarized in Fig. 3.

Four useful inferences can be drawn from these seismic velocity profiles. First, the average Vp/Vs (1.78) indicates an intermediate bulk crustal composition, perhaps indicating mixtures of mafic and felsic lithologies at many scales within the crust. There is some variability in the Vp/Vs ratios between the stations, but given their uncertainties they are not much different. Second, Eastern Desert crustal thickness appears to be significantly (~30%) less than normal typical continental crust. Crustal thickness – defined by the depth to Vs = 4.3 km/s - is 28 km beneath HRG, NABD, and BRNS and 33 km beneath BRNS. Normal continental crust is generally ~40 km thick. It is not clear why Eastern Desert crust is so much thinner than normal continental crust. An additional constraint is the low metamorphic grade of many Eastern Desert supercrustal sequences, for example the Hammamat Group. This suggests that there has not been a lot of erosion since the end of Precambrian time, so the observed crustal thickness could have been established at that time or by delamination loss of ~10 km of mafic lower crust associated with Red Sea opening. It is more likely that this thickness was established by mid-Ediacaran time (~600 Ma), when a regional episode of delamination is suggested to have occurred (Avigad and Gvirtzman, 2009). A third point is that there is no obvious subdivision of slower upper crust on faster upper crust, as seen for normal continental crust including that of the Arabian Shield (Mooney et al., 1985). The high Vs zones in the upper crust beneath MRS, BRN and NABD perhaps indicate large mafic intrusions. Finally, there is evidence of a mafic underplate that is ~5 km thick. By analogy with the thicker mafic lower crust of the Arabian Shield, this may have formed ~600 Ma and been responsible for heating the infrastructure and providing fluids, as discussed below.

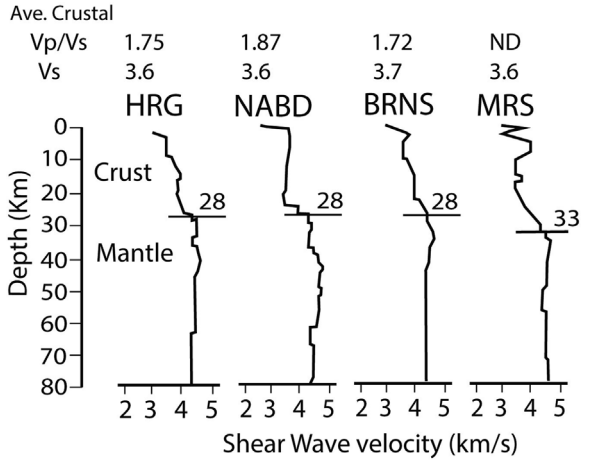

Fig. 3. Shear wave velocity models for the four Eastern Desert seismic stations (HRG). (NADB), (BRNS) and (MRS) (Locations shown in Fig. 1E. HRG is near Hurgada on the Red Sea coast (broadband station, VBB). NABD is in the Abou Dabbab area (VBB). MRS is located in Mars Alam area near the Red Sea coast south of the NABD station (SP station). BRNS is near Berenice in southern Egypt, inland and away from the Red Sea coast (VBB station). The Moho is taken to be where Vs reaches 4.3 km/s.

Fig. 4 presents a simplified version of our present understanding of Eastern Desert lithospheric composition, based on the above considerations coupled with the results of xenolith studies for Arabia (not possible for the Eastern Desert) as summarized by Stern and Johnson (2010).

4. Infrastructure

As discussed above, the overall vertical structure of the middle to upper crust in the CED and SED consists of a deformed, ophiolite-dominated superstructure on top of gneissic infrastructure, and this relationship is best seen in the CED. Infrastructure is migmatitic, gneissic, amphibolitic, and granodioritic. The boundary between Tier 1 superstructure and Tier 2 infrastructure is sometimes a low-angle shear associated with mylonitic gneisses and granites and sometimes is intruded by granite and granodiorite. The exhumation of ANS infrastructure at several localities (Meatiq, Migif-Hafafit, El-Sibai, El Shallul, and Betian) reflect interaction of Najd strike-slip shearing with hot and/or partially molten infrastructure. Examples of infrastructure geology and relations with surrounding supracrustal rocks are shown by the Meatiq and Hafafit domes (Fig. 5). These two examples show the heterogeneity of ED infrastructure, with more mafic rocks in the Hafafit exposures and abundant quartz-rich metasediments at Meatiq.

Eastern Desert infrastructure shows significant age variations from north to south, as summarized in Fig. 6. U-Pb zircon ages, take to approximate the time of crystallization and cooling below ~800 °C (Carlson, 2011) are oldest in the south (~720 Ma at Beitan) and young northward, with the youngest ages found in the northernmost exposure (~600 Ma at Meatiq), adjacent to the NED, which was an igneous hotspot ~600 Ma. These ages tell us when the lithosphere – especially its lower crust – was hot, partially molten, and weak. A variety of cooling ages – with blocking temperatures that range from ~600 °C (Sm-Nd garnet) to ~300 °C (Ar-Ar and Rb-Sr on mica; Carlson, 2011) - range from ~620 to ~570 Ma. These temperatures are well below the solidus of silicate rocks and so indicate when the lithosphere of a given region became strong; by this measure, Eastern Desert crust became essentially rigid by ~580 Ma. Fig. 8 summarizes how lithospheric strength varies as a function of temperature. The transformation of the middle and lower crust from exceptionally weak to strong over Cryogenian and Ediacaran time progressively northward exerted a strong control on how Najd shearing was manifested in the Eastern Desert.

Hot temperatures in the infrastructure probably were due to mafic underplating. Depending on the flux of mafic magma from

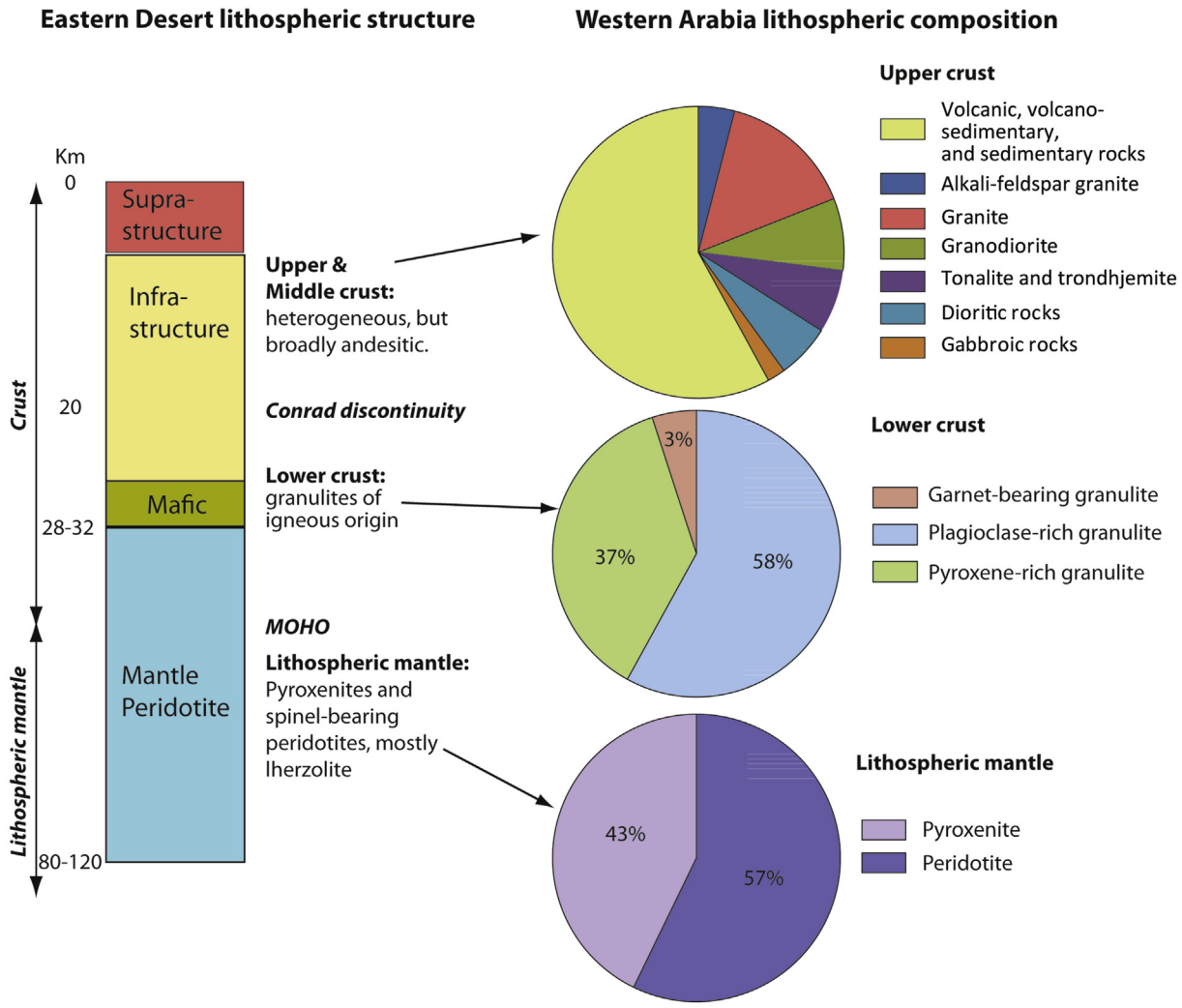

Fig. 4. Structure of the lithosphere beneath the Eastern Desert of Egypt, based on geophysical studies by Hosny and Nyblade (2016) modified by studies of crustal and upper mantle xenoliths from harrats (Cenozoic basalts) of western Arabia, summarized by Stern and Johnson (2010). Three pie diagrams show estimates of upper continental crust, lower crust, and lithospheric mantle, based on Arabian Shield surface exposures for upper crust and from xenoliths in Cenozoic lavas of Arabia for lower crust and lithospheric mantle. For upper crust, gneiss is calculated in terms of the protolith — thus dioritic gneiss is grouped with diorite; granite gneiss with granite, etc. Ophiolitic rocks are not included. Dashed line suggests that contact between infrastructure and superstructure may be deeper in places, based on P-T studies discussed in text. Composition of western Arabian lithosphere, as determined from outcrops for upper crust (after Johnson et al., 2011), which is similar to that of the Eastern Desert of Egypt. Also shown are reported proportions of lower crust and lithospheric mantle xenoliths brought up in Neogene volcanic eruptions in western Arabia (Stern and Johnson, 2010), which is a reasonable approximation for the mantle beneath the Eastern Desert of Egypt.

the mantle, such a magmatic "hot zone" of the sort described by Annen et al. (2006) could be established in a few million years. Because terminal collision between E and W Gondwana began ~630 Ma (Stern, 1994), arc magmas would have dominated early basaltic underplated magmas and influenced formation of infrastructure in the older domes (Beitan, Hafafit, and El Sibai), whereas post-collisional within-plate basaltic underplates influenced formation of <630 Ma crustal melts. The overall evolution of igneous rocks during this transition, from older, calc-alkaline, I-type, and hydrous to younger, alkali, A-type, and anhydrous has been documented in Sinai (Eyal et al., 2010) and a similar evolutionary trend is consistent with Eastern Desert granitic rocks. The changing nature of underplating magmas has important implications for crustal fluids; early mafic magmas related to subduction are likely to have been rich in water but late mafic magmas are likely to have been rich in carbon dioxide. Studies of fluid inclusions in well-dated Eastern Desert plutonic rocks are needed to test this possibility.

Because of their relative high metamorphic grades and their schistose or gneissic fabrics, Eastern Desert infracrustal rocks were earlier interpreted as remnants of pre-Neoproterozoic continental crust (e.g., Habib et al., 1985; El Gaby et al., 1988, 1990). However, everywhere that geoscientists have been able to obtain reliable U-Pb zircon ages, these rocks are Neoproterozoic, as summarized in Fig. 6, without xenocrystic zircons of greater age. Determinations of the initial isotopic composition of Sr, Nd, Pb, or Hf for Eastern Desert infrastructure rocks also show the distinctive isotopic composition expected for Neoproterozoic mantle or can be explained by remelting of juvenile volcanics (Liégeois and Stern, 2010). The juvenile (mantle-derived) nature of supracrustal igneous rocks has already been discussed, and the geochronologic and isotopic data for infrastructure rocks also is further evidence that Eastern Desert crust in its entire thickness was entirely produced by mantle melting of Neoproterozoic mantle, with further processing by fractionation and remelting in this juvenile Neoproterozoic crust.

In spite of abundant evidence to the contrary, some geoscientists — mostly Egyptian - persist in believing that Eastern

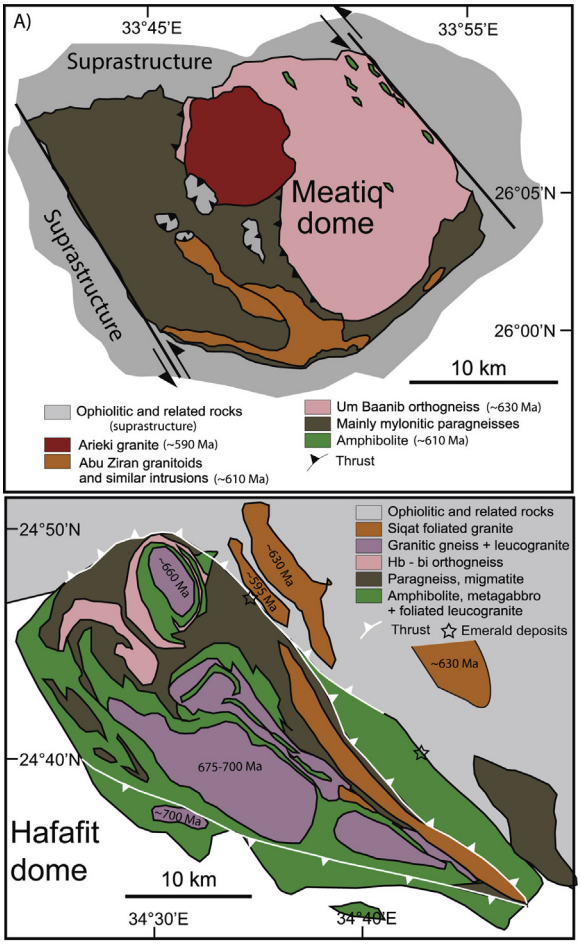

Fig. 5. Simplified geological map for the Meatiq (A) and Hafafit domes. (B). Colored units are distinguishable units in the crustal infrastructure. Maps are modified after Liégeois and Stern (2010). Also shown are approximate U-Pb zircon ages for Meatiq from Andresen et al. (2010) and Stern and Hedge (1985) and for Hafafit from Lundmark et al. (2012) and Kröner et al. (1994). Approximate emerald deposit localities are from Grundmann and Morteani (2008). (For interpretation of the references to colour in this figure legend, the reader is referred to the web version of this article.)

Desert infrastructure may be Archean or Paleoproterozoic "fundamental basement". These skeptics must demonstrate the existence of such remnants using modern and reliable tools. Modern geochronology and isotope geochemistry has failed to find any evidence in support of this old idea; even geoscientists who continue to argue for the involvement of pre-Neoproterozoic crust in the infrastructure acknowledge that these isotopic compositions are overwhelmingly mantle-like (Khudeir et al., 2008), and show very little if any evidence for the involvement of pre-Neoproterozoic crust. The situation for the Eastern Desert contrasts with what modern approaches yield for Sinai basement. Basement rocks with ~1.0 Ga U-Pb zircon ages are documented from the Sa'al region (Be'eri-Shlevin et al., 2012). Abu El-Enen and Whitehouse (2013) carried out U-Pb zircon dating of 14 samples of orthogneiss, paragneiss, and granitic rocks from the Feiran-Solaf gneiss belt (~50 km west of Sa'al). They found that 4 samples preserved compelling evidence of ~1.0 Ga zircons in the infrastructure, even though the region was later affected by four major melting episodes at ~800 Ma, ~700 Ma, ~620 Ma, and ~600 Ma. For this reason, it seems likely that if significant tracts of pre-Neoproterozoic crust exist in the Eastern Desert, there should be compelling geochronologic or isotopic evidence for this. The one place where there is some U-Pb zircon evidence for pre-Neoproterozoic ages in the Eastern Desert infrastructure is at Sikait, east of Migif-Hafafit, where Abdel-Monem and Hurley (1979) reported a very discordant U-Pb zircon age ~1770 Ma. It would be very useful to undertake a careful study of infrastructure rocks around the Zabara, Sikait, and Umm Kabo emerald deposits, emphasizing careful mapping and collection of samples for geochronological and isotopic studies.

Some of the infrastructure domes (Meatiq, Migif-Hafafit, El-Sibai, El Shallul, and Beitan) have been studied to reconstruct their pressures and temperatures of equilibration; these are summarized in Fig. 7. Amphibolites of the Meatiq Dome show maximum P ~8 kbar and T ~750 °C (Neumayr et al., 1998; Fritz et al., 2002). This P corresponds to ~26 km deep in the crust. Similarly, Hafafit gneisses experienced peak metamorphic conditions of ~7 kbar (corresponding to ~23 km deep) and T ~650 °C (Abd El-Naby et al., 2008). Bregar et al. (2002) observed similar geologic relationships around the El-Sibai dome SE of Meatiq. The Sibai magmatic core complex consists of strongly deformed gneisses with (amphibolite lenses) and associated granitic rocks (infrastructure) that are tectonically separated from surrounding rocks of the ensimatic assemblage (superstructure). Similar P-T estimates are made for exposed infrastructure in the Feiran-Solaf metamorphic complex in Sinai, where Abu-Alam and Stüwe (2009) estimated peak metamorphic conditions of 700–750 °C and 7–8 kbar. Similar estimates come from ANS exposures in NW Arabian Shield, where Meyer et al. (2014) studied infrastructure-superstructure relations exposed in a Najd-related gneiss dome around the Qazaz dome. They used the hornblende-plagioclase thermometer and Al-in-hornblende barometer to estimate peak metamorphic conditions of 560–640 °C and pressures of 7.5 ± 0.5 kbar for a gneiss in the core of the dome and 570–630 °C and 7.0 ± 0.5 kbar for a gneiss on the periphery of the dome, indicating that this gneiss rose up from ~23 to 24 km deep in the crust; nearby sediments of the Thalbah Group are very similar to the Hammamat and demonstrate that gneiss exhumation occurred in Ediacaran time, associated with Najd shearing.

Fig. 7 summarizes the typical clockwise P–T paths of Eastern Desert infrastructure exposures. These cooling paths are interpreted by Fritz et al. (2013) as resulting from advective heat transport induced by magma emplacement together with exhumation. In contrast, rocks of the superstructure were subjected to significantly lower T and P. Ophiolitic rocks around the Meatiq dome show a maximum P ~4 kbar and ~450 °C (Fritz et al., 2002). Superstructure rocks around the El-Sibai core complex were metamorphosed at 480–525 °C and 2–4.5 kbar (6.6–15 km; Abd El-Wahed, 2008). A schist sample from west of the Qazaz dome reached peak conditions of 400–460 °C and 4.4–5.0 kbar (15.5–17.5 km depth; Meyer et al., 2014). A sample of Thalbah group (probable Hammamat equivalent) from ~120 m distant from the Qazaz shear zone reached 450 °C and 0.7 ± 0.2 kbar (depth ~1.6–3.2 km).

In summary, these studies indicate markedly different P-T environments for Eastern Desert infrastructure and superstructure, with P-T estimates of 7–8 kbar and 560–750 °C for gneissic infrastructure and 2–5 kbar and 400–500 °C for greenschist-facies superstructure. This further indicates that the boundary between infrastructure and superstructure is marked by a telescoped thermal gradient that is sometimes a mylonite zone and sometimes an intrusive contact, essentially juxtaposing hot, partially molten, ductile middle and lower crust with cooler, brittle upper crust. This telescoped temperature gradient represents a rheological boundary of fundamental significance to understanding the evolution of the Eastern Desert and its economic potential, as discussed in the next section.

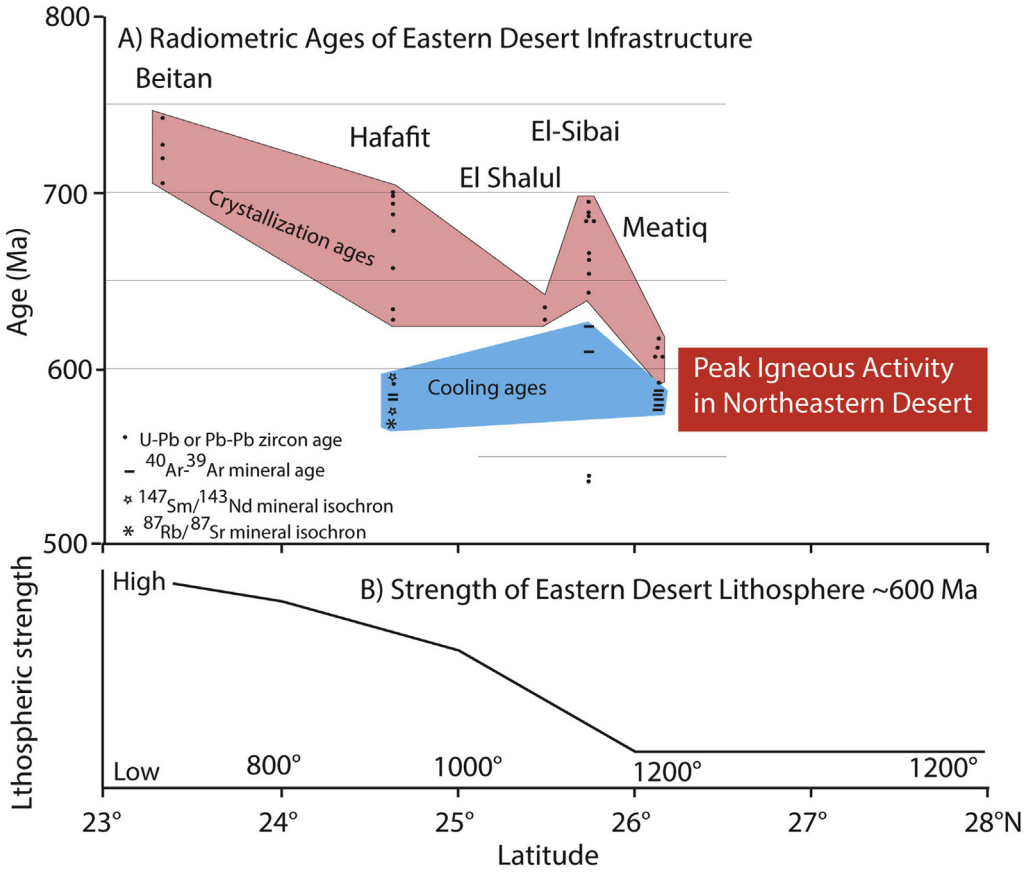

Fig. 6. A) U-Pb zircon crystallization ages (in pink) and various cooling ages ($^{40}Ar/^{39}Ar$, $^{143}Nd/^{147}Sm$, and $^{87}Sr/^{87}Rb$ mineral ages, in blue) for the five exposures of infrastructure in the Eastern Desert of Egypt. Note overall trend of younger crystallization ages northward, with ages in the northernmost complex being indistinguishable from peak igneous activity in the NE Desert ~600 Ma. Data sources are given in Table 1. B) Simplified summary of strength of Eastern Desert lithosphere ~600 Ma, based on thermal situation as summarized in A) and considerations encapsulated in Fig. 8. Estimated moho temperatures ~600 Ma are given in °C at bottom of figure. (For interpretation of the references to colour in this figure legend, the reader is referred to the web version of this article.)

Lithospheric strength is likely to have varied significantly beneath the Eastern Desert ~600 Ma. The reasons for this are summarized in Fig. 8, which graphically shows that lithospheric strength reflects its thermal structure. Hot lithosphere is much weaker than cold lithosphere. Regional deformation (strain) is preferentially concentrated where lithosphere is weakest. At ~600 Ma, when Najd shearing and NE Desert extension occurred, this deformation would naturally have been concentrated where the lithosphere was hottest and weakest, in the NED and northern CED. At this time the moho beneath the NED and northern CED was probably ~1000 °C due to mafic underplating whereas the southern CED and SED was probably cooler and stronger. It is also important to note that steep Najd faults at this time would only be preserved in cool superstructure and deformation in partially molten infrastructure would not preserve such structures. Najd shears are likely to have flattened near the boundary with partially molten infrastructure. The nature of the deforming contact between infrastructure and superstructure played an important role in concentrating fluids at this important rheological boundary ~600 Ma.

A final point is that the base of the superstructure is dominated by serpentinized ophiolitic ultramafics, and there is an opportunity to use these to reconstruct superstructure thermal structure. Serpentinites come in three varieties: lizardite, chrysotile, and antigorite and differ in terms of their T stability. Lizardite and chrysotile are stable at T up to 300–400 °C whereas antigorite is stable up to ~600 °C (Evans, 2004). These varieties of serpentinite have been documented in the Eastern Desert (Surour, in press; Boskabadi et al., in press). It is likely that the lower parts of the superstructure were more heated than the upper parts, so the distribution of these serpentinite varieties in the Eastern Desert might reveal how close different serpentinite outcrops are to the infrastructure, with antigorite dominating the lower superstructure and lizardite-chrysotile dominating higher up. An important step forward would be to better understand what is the distribution of these varieties of serpentinite in the Eastern Desert, and whether or not these varieties are organized systematically.

5. Fluid transport and the Eastern Desert Decollement

As noted above, a major, boundary separates infrastructure and superstructure, and this boundary was tectonically active ~600 Ma. The boundary between these two realms was due to movement on the subhorizontal shear zone (Meyer et al., 2014), at least late in its development ~600 Ma; we don't know when it formed. The shear zones form a system of crustal dislocations referred to as the Eastern Desert Shear Zone (EDSZ) (Andresen et al., 2009, 2010). The EDSZ originated as a subhorizontal shear zone but was subsequently deformed so that exposures are often subvertical. The EDSZ is related to ~600 Ma Najd faulting, as shown by consistent NW-SE oriented mineral lineations in the CED and adjacent regions (Ries et al., 1983; Loizenbauer et al., 2001; Abd El-Wahed, 2008; Shalaby, 2010; Meyer et al., 2014). It may be useful to rename the infrastructure-superstructure boundary as the Eastern Desert

Table 1
Radiometric age constraints for Five Eastern Desert Infrastructure Exposures

Region	Latitude	Lithology and name	Infras/super	Age	Technique	Reference
Meatiq	26.1	Felsite	super	748 ± 3	U-Pb zirk TIMS	Andresen et al., 2009
Meatiq	26.1	Fawakhir ophiolite	super	737 ± 1	U-Pb zirk TIMS	Andresen et al., 2009
Meatiq	26.1	Abu Ziran diorite	infra	606 ± 1	U-Pb zirk TIMS	Andresen et al., 2009
Meatiq	26.1	Arieki granite	infra	590 ± 3	U-Pb zirk TIMS	Andresen et al., 2009
Meatiq	26.1	Diorite lense 1	infra	609 ± 1	U-Pb zirk TIMS	Andresen et al., 2009
Meatiq	26.1	Diorite lense 2	infra	606 ± 1	U-Pb zirk TIMS	Andresen et al., 2009
Meatiq	26.1	Um Baanib Gneiss 1	infra	570 ± 0.3	Hb 40/39	Fritz et al., 2002
Meatiq	26.1	Um Baanib Gneiss 2	infra	581 ± 0.2	Hb 40/39	Fritz et al., 2002
Meatiq	26.1	Um Baanib Gneiss 3	infra	579 ± 0.2	Hb 40/39	Fritz et al., 2002
Meatiq	26.1	Um Baanib Gneiss 4	infra	584 ± 0.2	Hb 40/39	Fritz et al., 2002
Meatiq	26.1	Metapelite (garnet-kyanite schist)	infra	582 ± 0.2	Msc 40/39	Fritz et al., 2002
Meatiq	26.1	Abu Ziran granodiorite	infra	614 ± 8	U-Pb zirc. Conv.	Stern and Hedge, 1985
El-Sibai	25.75	Amphibolite lense	infra	607 ± 0.2	Hb 40/39	Fritz et al., 2002
El-Sibai	25.75	Abu Markhat gneiss	infra	624 ± 0.2	Hb 40/39	Fritz et al., 2002
El-Sibai	25.75	AA07-16 El-Shush granodiorite	infra	682 ± 4	U-Pb zirk TIMS	Augland et al., 2012
El-Sibai	25.75	AA07-17 El-Shush granitic gneiss	infra	679 ± 2	U-Pb zirk TIMS	Augland et al., 2012
El-Sibai	25.75	AA07-18 El-Shush coarse granitic gneiss	infra	685 ± 3	U-Pb zirk TIMS	Augland et al., 2012
El-Sibai	25.75	AA07-25 Umm Gheigh anorthosite	infra	541 ± 2	U-Pb zirk TIMS	Augland et al., 2012
El-Sibai	25.75	AA07-26 Um Gheigh syenogranite dike	infra	540 ± 1	U-Pb zirk TIMS	Augland et al., 2012
El-Sibai	25.75	KP273 El Shush gneiss	infra	694 ± 27	zirc evap	Bregar et al., 2002
El-Sibai	25.75	MP320 El Shush gneiss	infra	679 ± 7	zirc evap	Bregar et al., 2002
El-Sibai	25.75	MB184 Central gneiss	infra	659 ± 14	zirc evap	Bregar et al., 2002
El-Sibai	25.75	AB281 granite	infra	645 ± 5	zirc evap	Bregar et al., 2002
El-Sibai	25.75	ED151 granite	infra	653 ± 15	zirc evap	Bregar et al., 2002
El-Sibai	25.75	MB195 granite	infra	657 ± 24	zirc evap	Bregar et al., 2002
Hafafit	24.6	orthogneiss	infra	586 ± 0.3	Hb 40/39	Fritz et al., 2002
Hafafit	24.6	orthogneiss	infra	584 ± 0.2	Hb 40/39	Fritz et al., 2002
Hafafit	24.6	EG 27 granitoid gneiss	infra	700 ± 12	zirc evap	Kröner et al., 1994
Hafafit	24.6	EG28 granitoid gneiss	infra	698 ± 14	zirc evap	Kröner et al., 1994
Hafafit	24.6	EG30 granitoid gneiss	infra	677 ± 9	zirc evap	Kröner et al., 1994
Hafafit	24.6	7-81 tonalite	infra	682 ± 2	U-Pb zirc. conv.	Stern and Hedge, 1985
Hafafit	24.6	Nugrus	infra	591 ± 4	U-Pb zirk TIMS	Lundmark et al., 2012
Hafafit	24.6	Hangalia	infra	629 ± 5	U-Pb zirk TIMS	Lundmark et al., 2012
Hafafit	24.6	Zabara	infra	633 ± 5	U-Pb zirk TIMS	Lundmark et al., 2012
Hafafit	24.6	El Sukkari	infra	689 ± 3	U-Pb zirk TIMS	Lundmark et al., 2012
Hafafit	24.6	Migmatitic tonalite gneiss	infra	659 ± 5	U-Pb zirk TIMS	Lundmark et al., 2012
Hafafit	24.6	H18 Biotite Gneiss	infra	573 ± 6	Rb-Sr internal	Abd El-Naby et al., 2008
Hafafit	24.6	H19 Amphibolite	infra	585 ± 8	Sm-Nd internal	Abd El-Naby et al., 2008
Hafafit	24.6	H23 Hornblende Gneiss	infra	593 ± 4	Sm-Nd internal	Abd El-Naby et al., 2008
Beitan	23.3	EG747	infra	704 ± 8	zirc evap	Kröner et al., 1994
Beitan	23.3	WB21 tonalitic gneiss	infra	719 ± 10	zirc SIMS	Ali et al., 2015
Beitan	23.3	WB23 granodiritic gneiss	infra	725 ± 9	zirc SIMS	Ali et al., 2015
Beitan	23.3	WB24 tonalitic gniss	infra	744 ± 10	zirc SIMS	Ali et al., 2015
El Shalul	25.5	SH1 granite	infra	637 ± 5	zirc LA-ICP-MS	Ali et al., 2012
El Shalul	25.5	SH6 granitic gneiss	infra	631 ± 6	zirc LA-ICP-MS	Ali et al., 2012

Decollement (EDD) in order to emphasize its origins as a predominantly subhorizontal shear zone (Fig. 9).

The rheological contrast marked by the EDD and the strain gradient that it represented when it was deforming played key roles in concentrating fluids and melts. This was for three reasons. First, fluids had different sources in the infrastructure and superstructure. The infrastructure remained partially molten as long as mafic magma continued to be added to the base of the crust. Volatiles (especially CO_2 and H_2O) released from mafic underplating magma flowed upwards through the infrastructure towards the EDD (Fig. 9). In contrast, some fluids in the superstructure originated as meteoric (surface and near-surface) water and flowed downward towards the EDD. Breakdown of hydrous minerals in infrastructure (biotite and hornblende) and superstructure (serpentine) also contributed to the fluid budget. Second, the EDD separated two different rheological regimes, ductile in the infrastructure and brittle in the superstructure. Deformation favored alteration and alteration weakened the rocks, further concentrating strain. We do not know what fluid pressures were on the EDD but if overpressuring occurred there, this would have further favored movement there. Third, the EDD corresponded to a major change in thermal regime, from hot infrastructure – dominated by ductile deformation – to overlying cooler infrastructure, where deformation was mostly brittle, with fracturing favoring fluid flow.

We have some information about the nature of Eastern Desert fluids as they existed ~600 Ma. Evidence for fluid involvement in infrastructure was reported by Loizenbauer et al. (2001), who documented three generations of fluid inclusions in Meatiq gneisses. The first generation is dominated by H_2O and CO_2 whereas the second generation consists of two assemblages: $CO_2 + H_2O$-rich and CO_2-rich. Fluid inclusions with constant X_{CO2} (0.5–0.7) were documented from the eastern and western strike-slip (Najd) shear zones. Loizenbauer et al. (2001) found similar fluid inclusions in the associated ophiolitic rocks. These fluid inclusions are often aligned parallel to shear zones and boudins, suggesting that at least some of the fluid migrated during deformation.

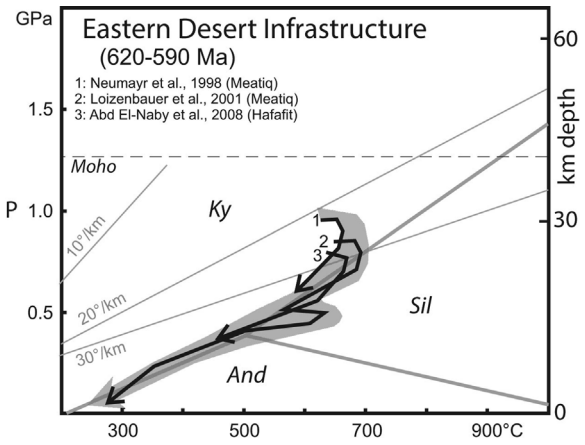

Fig. 7. Summary of P-T studies for Eastern Desert infrastructure, modified after Fritz et al. (2013). Also shown are linear geothermal gradients and stability fields of kyanite (Ky), sillimanite (Sil), and andalusite (And) are indicated. Grey shaded arrow shows average trend.

The origins and effects of the carbonate-rich fluids in Eastern Desert superstructure are particularly interesting. The origin of these fluids has been studied by Stern and Gwinn (1990), who focused and massive carbonate intrusive bodies. They used C, O, and Sr isotopic data to identify three distinct reservoirs for these bodies: (1) sedimentary carbonates, with moderately high $^{87}Sr/^{86}Sr$ and heavy C and O; (2) depleted mantle, with low $^{87}Sr/^{86}Sr$ and light C and O; and (3) enriched mantle or lower crust, with high $^{87}Sr/^{86}Sr$ and light C and O. Isotopic data indicate that the intrusive carbonates of the North Eastern Desert were derived from reservoir (2). The origin of other intrusive carbonates of the Central Eastern

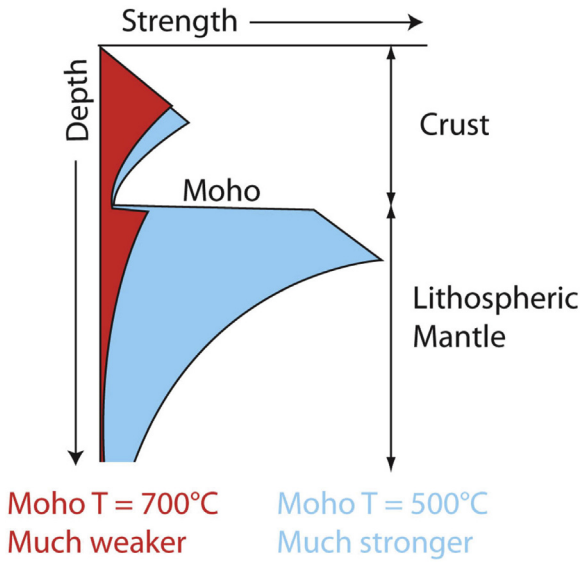

Fig. 8. Simplified yield strength profiles showing how lithospheric strength depends on temperature. Crust is modeled using quartz rheology, mantle is modeled using olivine rheology. Total lithospheric strength is area to the left of curve. Linear increase of strength with depth follows Byerlee's Law (Byerlee, 1968) from the surface down until the brittle-ductile transition, below which the rocks are hotter and strength is determined by strain rate and temperature (Brace and Kohlstedt, 1980). The two simplified strength profiles have conductive geothermal gradients; note the much greater strength of lithosphere where moho T = 500 °C compared to the case where moho T = 700 °C. See text for discussion of how the different strength of lithosphere beneath different parts of the Eastern Desert controlled many aspects of its evolution in Ediacaran time.

Desert and Sudan is best explained as due to mixing between remobilized sedimentary carbonates and mantle fluids, i.e. reservoirs (1) and (2).

Similar carbonate-rich fluids pervasively altered ED ophiolitic ultramafics, which were mostly highly serpentinized harzburgites. Boskabadi et al. (in press) studied lizardite serpentinites, antigorite serpentinites, and listvenitic rocks associated carbonate and quartz veins around the Meatiq dome. C, O and Sr isotopes of vein samples cluster between −8.1‰ and −6.8‰ $\delta^{13}C$, +6.4‰ to +10.5‰ $\delta^{18}O$, and $^{87}Sr/^{86}Sr$ of 0.7028–0.7034, and plot within the depleted mantle compositional field. The Lz- and Atg-serpentinite isotopic compositions reflect mixing between the depleted-mantle and sedimentary carbonate fields. Carbonate vein rocks contain abundant carbonic (CO_2±CH_4±N_2) and aqueous-carbonic (H_2O-NaCl-CO_2±CH_4±N_2) low salinity fluid inclusions, with trapping conditions of 270 °C–300 °C and 0.7–1.1 kbar (2.5–4 km deep in the crust).

There is strong evidence that gold mineralization and carbonate fluid infiltration in the ED were intimately related. Fluid inclusion and stable isotope compositions of CED Au deposits are similar to those from the carbonate veins. Boskabadi et al. (in press) suggest that carbonation of ANS ophiolitic rocks due to influx of mantle-derived CO_2-bearing fluids broke down Au-bearing minerals such as pentlandite, releasing Au and S infiltrating fluids that later formed the Au-deposits. Mineralized quartz veins may be related to remobilization of silica due to conversion of olivine-rich peridotites (40 wt % SiO_2) into talc-rich (30 wt % SiO_2) by reactions with carbonate fluid. Illuminating in this regard is the listvenite gold mineralization of Barramiya (CED; Zoheir and Lehmann, 2010). Gold-bearing quartz veins are associated with carbonaceous, listvenitized serpentinite and adjacent to post-tectonic granite stocks. Mineralized quartz veins contain abundant carbonic (CO_2±CH_4±H_2O) and aqueous-carbonic (H_2O–NaCl–CO_2±CH_4) inclusions. Based on the fluid inclusions data combined with thermometry of arsenopyrite, Zoheir and Lehmann (2010) estimated that the pressure–temperature conditions of mineralization ranged from 1.3 to 2.5 kbar (4–7 km deep in the crust) at 325–375 °C. $\delta^{34}S$ values of sulfides range from −5.6 to +3.2, bracketing the mantle value $\delta^{34}S$–0 (Zoheir and Lehmann, 2010). Zoheir and Lehmann (2010) suggested that the ore fluids infiltrated into the sheared listvenite rocks, where interaction with carbonaceous wallrocks lowered fluid fO_2 and triggered gold deposition.

Similar results were found for shear zone-related, mesothermal gold deposits of Um Egat and Dungash in the ED south of Barrimaya (Zoheir et al., 2008). The gold deposits are hosted by greenschist facies metavolcanic and/or metasedimentary superstructure sequences. Both deposits comprise boudinaged quartz veins containing pyrite, arsenopyrite ± pyrrhotite ± chalcopyrite ± galena; gold occurs is usually included in arsenopyrite, pyrite, or pyrrhotite next to fragments of altered country rocks, or disseminated in alteration haloes. Arsenic in arsenopyrite and Aliv in chlorite geothermometers indicate that wall-rock alteration and ore mineral precipitation occurred at temperatures between 400° and 250 °C. Three types of fluid inclusions were identified based on petrography and laser micro-Raman spectroscopy: (1) two-phase carbonic inclusions with CO_2 + CH_4 ± N_2 ± H_2O, (2) two-phase aqueous inclusions, and (3) three-phase aqueous-carbonic inclusions with CH_4. Field, petrographic, and microthermometric data suggest that low-salinity aqueous-carbonic fluids interacted with graphite-bearing rocks in the superstructure to form CH_4 at T > 400 °C and P > 3 kbars, where supercritical conditions were likely. These reduced fluids leached gold as they circulated through the metavolcanic rocks, carrying it in the form of bisulfide complexes. Interaction of these aqueous-carbonic fluids with the country rocks caused hydrothermal alteration and precipitated

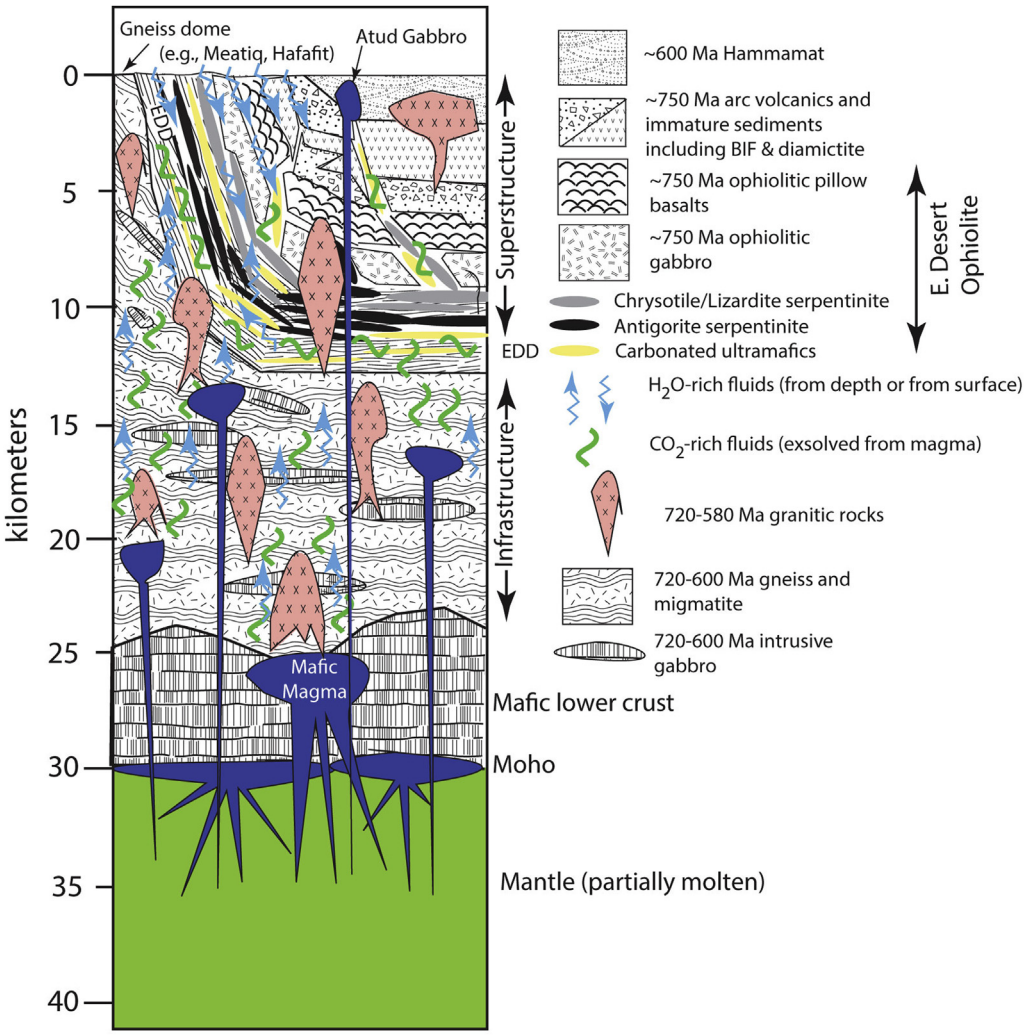

Fig. 9. Schematic diagram illustrating crustal structure and processes beneath the Central Eastern Desert ~600 Ma. Partial melting of upper mantle produces large volumes of mafic, volatile-rich, mafic magma. Volatile-rich magma is mostly underplated to the base of the crust but also is emplaced higher up in the infrastructure and small batches reach near the surface (Atud Gabbro). These magmas heat infrastructure amphibolites and gneisses to generate granitic melts. Mafic magmas release volatiles as they rise into the crust and crystallize. Hydrous fluids also circulate downward from the surface. Deformation is concentrated along the Eastern Desert Detachment (EDD) where fluids from depth and surface mix and alter sheared rocks, especially serpentinized harzburgites, carbonating them into talc-carbonate (listvenite).

gold-bearing sulfides in the alteration zones. A drop of pressure during the migration of these fluids to shallower depths along the shear zones led to phase separation at ~300 °C and P ~2.3 kbars (~7 km deep). Quartz crystallizing over a range of lower temperatures and pressures trapped carbonic and aqueous fluids as separate inclusions. Deformation remobilized the gold, depositing it as globules of higher fineness in secondary sites.

We do not yet have much geochronology for gold deposits of the Eastern Desert, but we have a Re-Os age of 601 ± 17 Ma for mineralization in the Fawkhir-El Sid gold deposit (Zoheir et al., 2014). We need more Re-Os ages for ED gold deposits.

Key insights into the nature of processes that occurred along the infrastructure-superstructure contact are provided by emerald deposits along the NE flank of the Migif-Hafafit dome, at Zabara, Sikait and Umm Kabo. Grundmann and Morteani (2008) noted that these deposits are concentrated along the sheared infrastructure-superstructure contact. They conducted detailed microstructural and chemical studies and noted the Cr- and Mg-rich composition of these emeralds, indicating a metamorphic origin. Grundmann and Morteani (2008) emphasized the local availability of Cr-, Mg- and Be-rich fluids during metamorphism, which accompanied Najd (~600 Ma) deformation. Emerald-rich quartz lenses demonstrate that those fluids mobilized silica as well.

6. Conclusions

We are starting to reconstruct the processes that contributed to the shaping of Eastern Desert crust, but there is much more fundamental research that is needed. The following are a few specific suggestions for future research.

1) We need more geophysical studies to understand ED crustal and lithospheric structure, including gravity, passive seismic (teleseismic) and active seismic (reflection to better understand its thickness and structure, particularly whether or not there is a velocity inversion in the crust. Seismic traverses across each of the three blocks are needed (NED, CED, and SED). Seismic data would be very useful for constraining gravity models for crustal density structure. We also need a magnetic map for the ED to better reveal structural trends.
2) We want to better understand the age and nature of the Ediacaran ED magmatic underplate. The Atud gabbros may

be representatives of this magmatic phase. Representative Atud gabbro intrusions should be studied and radiometrically dated to evaluate this possibility.

3) The origin of Late Tonian- Cryogenian clastic sediments in the CED is unresolved. Representative sections should be identified, mapped and studied carefully, including U-Pb zircon ages designed to constrain age and provenance.
4) The extreme north of the NED should be mapped, studied in the lab, and radiometrically dated to see if evidence for ~1 Ga crust like that in Sinai can be recognized.
5) The possibility of a Hammamat River, flowing from the NED into the NW part of the CED should be tested by careful field mapping and study of detritus, including U-Pb zircon ages.
6) Modern geochronological and isotopic studies should be carried out east of Migif-Hafafit, where Abdel-Monem and Hurley (1979) reported a very discordant ~1770 Ma U-Pb zircon age.
7) There is a pressing need to better understand the age and nature of SED crust. Specifically, we need more U-Pb zircon ages and radiometric isotope studies of well-characterized SED basement samples. Traverses may be a good way to accomplish this.
8) The origin and nature of fluids that altered the superstructure needs to be better characterized by a wide range of studies. We need more fluid inclusion studies and isotopic studies of the fluids and suitable altered rocks, especially serpentinites, to better understand how these interacted with ophiolitic harzburgites and what if any relationship these interactions had to gold mineralization.
9) The distribution of different serpentine mineral species in especially the CED needs to be better understood, and how this does or does not reflect proximity to the Eastern Desert Decollement. If there is any systematic evolution of fluids through the EDD, this needs to be worked out in better detail.
10) We need more Re-Os ages for well-mapped and documented ED gold deposits in order to understand the relationship between Najd deformation and gold mineralization. Focused studies to understand the origin of gold-bearing quartz veins and what if any relations these have to carbonic fluid infiltration are also needed.

In this way we can more firmly link fundamental research in crustal evolution to economic geology and better honor the important contributions of Prof. El Ramly to our understanding of the very interesting geology of the Eastern Desert of Egypt.

Acknowledgements

I am grateful for the opportunity to contribute to this special issue honoring Prof. El Ramly's many accomplishments. Thanks also for constructive reviews by two anonymous referees. This is UTD Geosciences contribution # XXX.

References

Abd El-Naby, H., Frisch, W., Siebel, W., 2008. Tectono-metamorphic evolution of the Wadi Hafafit culmination (central eastern desert, Egypt). Implication for neoproterozoic core complex exhumation in NE Africa. Geol. Acta 6, 293–312.
Abd El-Rahman, Y., Polat, A., Dilek, Y., Fryer, B.J., El-Sharkawy, M., Sakran, S., 2009a. Geochemistry and tectonic evolution of the Neoproterozoic incipient arc–forearc crust in the Fawakhir area, Central Eastern Desert of Egypt. Precambrian Res. 175, 116–134.
Abd El-Rahman, Y., Polat, A., Dilek, Y., Fryer, B.J., El-Sharkawy, M., Sakran, S., 2009b. Geochemistry and tectonic evolution of the neoproterozoic Wadi Ghadir ophiolite, eastern desert, Egypt. Lithos 113, 158–178.
Abd El-Rahman, Y., Polat, A., Dilek, Y., Kusky, T.M., El-Sharkawi, M., Said, A., 2012. Cryogenian ophiolite tectonics and metallogeny of the central eastern desert of Egypt. Int. Geol. Rev. 54, 1870–1884.
Abd El-Rahman, Y., Seifert, T., Gutzmer, J., Said, A., Hofmann, M., Gärtner, A., Linneman, U., 2017. The South UmMongul Cu-Mo-Au prospect in the Eastern Desert of Egypt: from a mid-Cryogenian continental arc to Ediacaran post-collisional appinite-high Ba-Sr monzogranite. Ore Geol. Rev. 80, 250–266.
Abd El-Wahed, M.A., 2008. Thrusting and transpressional shearing in the Pan-African nappe southwest El-Sibai core complex, Central Eastern Desert. Egypt J. Afr. Earth Sci. 50, 16–36.
Abdeen, M.M., Greiling, R.O., 2005. A quantitative structural study of late Pan-African compressional deformation in the Central Eastern Desert (Egypt) during gondwana assembly. Gondwana Res. 8, 457–471.
Abdel-Karim, A.-A.M., Ahmed, Z., 2010. Possible origin of the ophiolites of Eastern Desert, Egypt, from geochemical perspectives. Arab. J. Sci. Eng. 35, 115–143.
Abdel-Karim, A.-A.M., Ali, S., Helmy, H.M., El-Shafei, H.M., 2016. A fore-arc setting of the Gerf ophiolite, Eastern Desert, Egypt: evidence from mineral chemistry and geochemistry of ultramafites. Lithos 263, 52–65.
Abdel-Monem, A.A., Hurley, P.M., 1979. U-Pb Dating of Zircons from Psammitic Gneisses, Wadi Abu Rosheid-Wadi Sikiat Area, Egyptian, vol. 3. Institute of Applied Geology, King Abdulaziz University Jeddah, Bulletin, pp. 165–170.
Abdel-Rahman, A.M., Doig, R., 1987. The Rb–Sr geochronological evolution of the Ras Gharib segment of the northern Nubian Shield. J. Geol. Soc. Lond. 144, 577–586.
Abdelsalam, M.G., Liégeois, J.P., Stern, R.J., 2002. The saharan Metacraton. J. Afr. Earth Sci. 34, 119–136.
Abu-Alam, T.S., Stüwe, K., 2009. Exhumation during oblique transpression: the Feiran–Solaf region, Egypt. J. Metamorph. Geol. 27, 439–459.
Abu El-Enen, M.M., Whitehouse, M.J., 2013. The Feiran–Solaf metamorphic complex, Sinai, Egypt: geochronological and geochemical constraints on its evolution. Precambrian Res. 239, 106–125.
Ali, K.A., Stern, R.J., Manton, W.I., Kimura, J.-I., Khamis, H.A., 2009. Geochemistry, Nd isotopes, and U-Pb SHRIMP zircon dating of neoproterozoic volcanic rocks from the central eastern desert of Egypt: new insights into the ~ 750 Ma crust-forming event. Precambrian Res. 171, 1–22.
Ali, K.A., Azer, M.K., Gahlan, H.A., Wilde, S.A., Samuel, M.D., Stern, R.J., 2010. Age constraints on the formation and emplacement of neoproterozoic ophiolites along the Allaqi-Heiani suture, South Eastern Desert of Egypt. Gondwana Res. 18, 583–595.
Ali, K.A., Stern, R.J., Manton, W.I., Johnson, P.R., Mukherjee, S.K., 2010. Neoproterozoic Atud diamictite of the eastern desert of Egypt and northern Saudi Arabia: evidence of ~750 Ma glaciation in the Arabian-nubian shield? Int. J. Earth Sci. 99, 705–726.
Ali, K.A., Andresen, A., Stern, R.J., Manton, W.I., Omar, S.A., Maurice, A.E., 2012. U-Pb zircon and Sr-Nd-Hf isotopic evidence for a juvenile origin of the c 634 Ma El-Shalul Granite, Central Eastern Desert, Egypt. Geol. Mag. 149, 783–797.
Ali, K.A., Kröner, A., Hegner, E., Wong, J., Li, S.-Q., Gahlan, H.A., El Ela, F.F., 2015. U–Pb zircon geochronology and Hf–Nd isotopic systematics of Wadi Beitan granitoid gneisses, South Eastern Desert, Egypt. Gondwana Res. 27, 811–824.
Andresen, A., Abu El-Rus, M.A., Myhre, P.I., Boghdady, G.Y., Corfu, F., 2009. U-Pb TIMS age constraints on the evolution of the neoproterozoic Meatiq gneiss dome, eastern desert of Egypt. Int. J. Earth Sci. 98, 481–497.
Andresen, A., Augland, L.E., Boghdady, G.Y., Lundmark, A.M., El Nady, O.M., Hassan, M.A., El Rus, M.A., 2010. Structural constraints on the evolution of the Meatiq gneiss dome (Egypt), east-African orogen. J. Afr. Earth Sci. 57, 413–422.
Annen, C., Blundy, J.D., Sparks, R.S.J., 2006. The Genesis of Intermediate and silicic magmas in deep crustal hot zones. J. Pet. 47, 505–539.
Augland, L.E., Andresen, A., Boghdady, G.Y., 2012. U-Pb ID-TIMS dating of igneous and metaigneous rocks from the El-Sibai area: time constraints on the tectonic evolution of the Central Eastern Desert, Egypt. Int. J. Earth Sci. 101, 25–37.
Avigad, D., Gvirtzman, Z., 2009. Late-Neoproterozoic rise and fall of the northern Arabian-Nubian Shield: the role of lithospheric mantle delamination and subsequent thermal subsidence. Tectonophysics 477, 217–228.
Azer, M.K., Stern, R.J., 2007. Neoproterozoic (835-720 Ma) serpentinites in the eastern desert, Egypt: fragments of forearc mantle. J. Geol. 115, 457–472.
Azer, M.K., Samuel, M.D., Ali, K.A., Gahlan, H.A., Stern, R.J., Ren, M., Moussa, H.E., 2013. Neoproterozoic ophiolitic peridotites along the Allaqi-Heiani suture, South Eastern Desert, Egypt. Mineral. Petrol. 107, 829–848.
Bennett, G.D., Mosely, P., 1987. Tiered tectonics and evolution, eastern deser and Sinai, Egypt. In: Matheis, G., Schandelmeier, H. (Eds.), Current Research in African Earth Sciences. Balkema, Rotterdam, The Netherlands, pp. 79–82.
Be'eri-Shlevin, Y., Eyal, M., Eyal, Y., Whitehouse, M.J., Litvinovsky, B., 2012. The Sa'al volcano-sedimentary complex (Sinai, Egypt): a latest Mesoproterozoic volcanic arc in the northern Arabian Nubian Shield. Geology 40, 403–406.
Boskabadi, A., Pitcairn, I.K., Broman, C., Boyce, A., Teagle, D.A.H., Cooper, M.J., Azer, M.K., Mohamed, F.H., Stern, R.J., 2016. Carbonate alteration of ophiolitic rocks in the Arabian Nubian Shield of Egypt: sources and compositions of the carbonating fluid and implications for the formation of Au deposits. Int. Geol. Review (in press).
Brace, W.F., Kohlstedt, D.L., 1980. Limits on lithospheric stress imposed by laboratory experiments. J. Geophys. Res. Solid Earth 85, 6248–6252.
Bregar, M., Bauernhofer, A., Pelz, K., Kloetzli, U., Fritz, H., Neumayr, P., 2002. A late Neoproterozoic magmatic core complex in the Eastern Desert of Egypt: emplacement of granitoids in a wrench-tectonic setting. Precambrian Res. 118, 59–82.
Breitkreuz, C., Eliwa, H., Khalaf, I., El Gameel, K., Bühler, B., Sergeev, S., Larinov, A., Murata, M., 2010. Neoproterozoic SHRIMP U–Pb zircon ages of silica-rich dokhan volcanics in the north eastern desert, Egypt. Precambrian Res. 182,

163–174.
Bühler, B., Breitkreuz, C., Pfänder, J., Hofmann, M., Becker, S., Linnemann, U., Eliwa, H.A., 2014. New insights into the accretion of the Arabian-nubian shield: depositional setting, composition and geochronology of a mid-cryogenian arc succession (north eastern desert, Egypt). Precambrian Res. 243, 149–167.
Byerlee, J.D., 1968. Brittle-ductile transition in rocks. J. Geophys. Res. 73, 4741–4750.
Carlson, R.W., 2011. Absolute age determinations: radiometric. In: Gupta, Harsh K. (Ed.), Encyclopedia of Solid Earth Geophysics. Springer, pp. 1–8.
El Ramly, M.F., 1972. A new geological map for the basement rocks in the Eastern and southwestern deserts of Egypt. Geol. Surv. Egypt Ann. 9, 125–135.
El Gaby, S., List, F.K., Tehrani, R., 1988. Geology, evolution and metallogenesis of the Pan African bellt in Egypt. In: El Gaby, S., Greiling, R.O. (Eds.), The Pan African Belt of Northeast Africa and Adjacent Areas. Balkema, Rotterdam, pp. 17–68.
El Gaby, S., List, F.K., Tehrani, R., 1990. The basement complex of the Eastern Desert and Sinai. In: Rushdi, S. (Ed.), The Geology of Egypt. Balkema, Rotterdam, pp. 175–184.
El-Shazly, A.K., Khalil, K.I., 2014. Banded iron formations of Um Nar, Eastern Desert of Egypt: P-T-X conditions of metamorphism and tectonic implications. Lithos 196–197, 356–375.
Eliwa, H.A., Breitkreuz, C., Murata, M., Khalaf, I.M., Bühler, B., Itaya, T., Takahashi, T., Hirahara, Y., Miyazaki, T., Kimura, J.-I., Shibata, T., Koshi, Y., Kato, Y., Ozawa, H., Daas, M.A., El Gameel, K., 2014. SIMS zircon U–Pb and mica K–Ar geochronology, and Sr–Nd isotope geochemistry of Neoproterozoic granitoids and their bearing on the evolution of the north Eastern Desert, Egypt. Gondwana Res. 25, 1570–1598.
Evans, B., 2004. The serpentinite multisystem revisited: chrysotile is metastable. Int. Geol. Rev. 46, 479–506.
Eyal, M., Litvinovsky, B., Jahn, B.M., Zanvilevich, A., Katzir, Y., 2010. Origin and evolution of post-collisional magmatism: coeval Neoproterozoic calc-alkaline and alkaline suites of the Sinai Peninsula. Chem. Geol. 269, 153–179.
Farahat, E.S., 2010. Neoproterozoic arc–back-arc system in the Central Eastern Desert of Egypt: evidence from supra-subduction zone ophiolites. Lithos 120, 293–308.
Fowler, A., Osman, A.F., 2013. Sedimentation and inversion history of three molasse basins of the western Central Eastern Desert of Egypt: implications for the tectonic significance of Hammamat basins. Gondwana Res. 23, 1511–1534.
Fritz, H., Dallmeyer, D.R., Wallbrecher, E., Loizenbauer, J., Hoinkes, G., Neumayr, P., Khudeir, A.A., 2002. Neoproterozoic tectonothermal evolution of the Central Eastern Desert, Egypt: a slow velocity tectonic process of core complex exhumation. J. Afr. Earth Sci. 34, 137–155.
Fritz, H., Abdelsalam, M., Ali, K., Bingen, B., Collins, A.S., Fowler, A.R., Ghebreab, W., Hauzenberger, C.A., Johnson, P., Kusky, T., Macey, P., Muhongo, S., Stern, R.J., Viola, G., 2013. Orogen styles in The east African orogens: a review of the neoproterozoic to cambrian tectonic evolution. J. Afr. Earth Sci. 86, 65–106.
Gahlan, H.A., Arai, S., 2009. Carbonate-orthopyroxenite lenses from the neoproterozoic gerf ophiolite, South Eastern Desert, Egypt: the first record in the Arabian nubian shield ophiolites. J. Afr. Earth Sci. 53, 70–82.
Gahlan, H.A., Azer, M.K., Khalil, A.E.S., 2015. The neoproterozoic Abu Dahr ophiolite, South Eastern Desert, Egypt: petrological characteristics and tectonomagmatic evolution. Mineral. Petrol. 109, 611–630.
Goldring, D.C., 1990. Banded iron formation of Wadi Sawawin district, Kingdom of Saudi Arabia. Trans. Ins. Min. Metall (Sec. B Appl. Earth Sci. 99, B1–B14.
Grundmann, G., Morteani, G., 2008. Multi-stage emerald formation during Pan-African regional metamorphism: the Zabara, Sikait, Umm Kabo deposits, South Eastern Desert of Egypt. J. Afr. Earth Sci. 50, 168–187.
Habib, M.E., Ahmed, A.A., El Nady, O.M., 1985. Two orogenies in the Meatiq Area of the Central Eastern of the Central Eastern Desert, Egypt. Precambrian Res. 30, 83–111.
Hammer, P.T.C., Clowes, R.M., Cook, F.A., Vasudevan, K., van der Velden, A.J., 2010. The big picture: a lithospheric cross section of the North American continent. GSA Today 21 (6), 4–10.
Hosny, A., Nyblade, A., 2016. Crustal structure of Egypt from Egyptian national seismic network data. Tectonophysics 687, 257–267.
Johnson, P.R., Woldehaimanot, B., 2003. Development of the Arabian-nubian shield: perspectives on accretion and deformation in the northern east African orogen and the assembly of gondwana. In: Yoshida, M., Windley, B.E., Dasgupta, S. (Eds.), Special Publications 2003, vol. 206. Geological Society, London, pp. 289–325.
Johnson, P.R., Andresen, A., Collins, A.S., Fowler, A.R., Fritz, H., Ghebreab, W., Kusky, T., Stern, R.J., 2011. Late Cryogenian-Ediacaran History of the Arabian-Nubian Shield: a review of depositional, plutonic, structural, and tectonic events in the closing stages of the northern East African Orogen. J. Afr. Earth Sci. 10, 1–179.
Khalil, A.E.S., Azer, M.K., 2007. Supra-subduction affinity in the neoproterozoic serpentinites in the eastern desert, Egypt: evidence from mineral composition. J. Afr. Earth Sci. 49, 136–152.
Khudeir, A.A., Abu El-Rus, M.A., El-Gaby, S., El-Nady, O., Bishara, W.W., 2008. Sr–Nd isotopes and geochemistry of the infrastructural rocks in the Meatiq and Hafafit core complexes, Eastern Desert, Egypt: evidence for involvement of Pre-Neoproterozoic crust in the growth of Arabian-Nubian Shield. Isl. Arc 17, 90–108.
Kröner, A., Todt, W., Hussein, I.M., Mansour, I.M., Mansour, M., Rashwan, A.A., 1992. Dating of late Proterozoic ophiolites in Egypt and the Sudan using the single grain zircon evaporation technique. Precambrian Res. 59, 15–32.
Kröner, A., Krüger, J., Rashwan, A.A.A., 1994. Age and tectonic setting of granitoid gneisses in the Eastern Desert of Egypt and south-west Sinai. Geol. Rundsch 83, 502–513.
Liégeois, J.-P., Stern, R.J., 2010. Sr-Nd isotopes and geochemistry of granite-gneiss complexes from the Meatiq and Hafafit domes, Eastern Desert, Egypt: No evidence for pre-Neoproterozoic crust. J. Afr. Earth Sci. 57, 31–40.
Loizenbauer, J., Wallbrecher, E., Fritz, H., Neumayr, H., Khudeir, A.A., Kloetzli, U., 2001. Structural geology, single zircon ages and fluid inclusion studies of the Meatiq metamorphic core complex: implications for Neoproterozoic tectonics in the Eastern Desert of Egypt. Precambrian Res. 110, 357–383.
Lundmark, A.M., Andresen, A., Hassan, M.A., Augland, L.A., Boghdady, G.Y., 2012. Repeated magmatic pulses in The east African orogen in the Eastern desert, Egypt: an old idea supported by new evidence. Gondwana Res. 22, 227–237.
McKenzie, D., Daly, M.C., Priestley, K., 2015. The lithospheric structure of Pangea. Geology 43, 783–786.
Meyer, S.E., Passchier, C., Abu-Alam, T., Stüwe, K., 2014. A strike-slip core complex from the Najd fault system, Arabian shield. Terra Nova 26, 387–394.
Mooney, W.D., Gettings, M.E., Blank, H.R., Healy, J.H., 1985. Saudi Arabian seismic-refraction profile: a traveltime interpretation of crustal and upper mantle structure. Tectonophysics 111, 173–246.
Neumayr, P., Hoinkes, G., Puhl, J., Mogessie, A., Khudeir, A.A., 1998. The Meatiq dome (Eastern Desert, Egypt) a Precambrian metamorphic core complex: petrological and geological evidence. J. Metamorph. Geol. 16, 259–279.
Powell, J.H., Abed, A.A., Le Nidre, Y.-M., 2014. Cambrian stratigraphy of Jordan. GeoArabia 19, 81–134.
Ries, A.C., Shackleton, R.M., Graham, R.H., Fitches, W.R., 1983. Pan-African structures, opiolites and mélange in the Eastern Desert of Egypt: a traverse at 26°N. J. Geol. Soc. Lond. 140, 75–95.
Shackleton, R., 1994. Review of Late Proterozoic sutures, ophiolitic mélanges and tectonics of eastern Egypt and north-east Sudan. Geol. Rundsch 83, 537–546.
Shalaby, A., 2010. The northern dome of Wadi Hafafit culmination, Eastern Desert, Egypt: structural setting in tectonic framework of a scissor-like wrench corridor. J. Afr. Earth Sci. 57, 227–241.
Sims, P.K., James, H.L., 1984. Banded Iron-formation of late proterozoic age in the central eastern desert, Egypt: geology and tectonic setting. Econ. Geol. 79, 1777–1784.
Stern, R.J., 1981. Petrogenesis and tectonic setting of late Precambrian ensimatic volcanic rocks, Central Eastern Desert of Egypt. Precambrian Res. 16, 195–230.
Stern, R.J., 1985. The Najd fault system, Saudi Arabia and Egypt: a late precambrian rift-related transform system. Tectonics 4, 497–511.
Stern, R.J., 1994. Neoproterozoic (900-550 Ma) arc assembly and continental collision in The east African orogen. Annu. Rev. Earth Planet. Sci. 22, 319–351.
Stern, R.J., Gwinn, C.J., 1990. Origin of late precambrian intrusive carbonates, eastern desert of Egypt and Sudan: C, O and Sr isotopic evidence. Precamb. Res. 46, 149–272.
Stern, R.J., Hedge, C.E., 1985. Geochronologic constraints on late Precambrian crustal evolution in the Eastern Desert of Egypt. Am. J. Sci. 285, 97–127.
Stern, R.J., Johnson, P., 2010. Continental lithosphere of the Arabian Plate: a geologic, petrologic, and geophysical synthesis. Earth Sci. Rev. 101, 29–67.
Stern, R.J., Gottfried, D., Hedge, C.E., 1984. Late precambrian rifting and crustal evolution in the northeastern desert of Egypt. Geology 12, 168–171.
Stern, R.J., Kröner, A., Rashwan, A.A., 1991. A late Precambrian (~710 Ma) high volcanicity rift in the South Eastern Desert of Egypt. Geol. Rundsch. 80,155–80,170.
Stern, R.J., Ali, K.A., Liégeois, J.-P., Johnson, P., Wiescek, F., Kattan, F., 2010. Distribution and significance of pre-neoproterozoic zircons in juvenile neoproterozoic igneous rocks of the Arabian-nubian shield. Am. J. Sci. 310, 791–811.
Stern, R.J., Mukherjee, S.K., Miller, N.R., Ali, K., Johnson, P.R., 2013. Banded iron formation from the Arabian-nubian shield – implications for understanding neoproterozoic climate change. Precambrian Res. 239, 79–94.
Stern, R.J., Ali, K., Ren, M., Jarrar, G.H., Romer, R.L., Leybourne, M., Whitehouse, M.J., 2016. Cadomian (~560 Ma) crust buried beneath the northern Arabian peninsula: mineral, chemical, geochronological, and isotopic constraints from NE Jordan xenoliths. Earth Planet. Sci. 436, 31–42.
Sultan, M., Arvidson, R.E., Sturchio, N.C., 1986. Mapping of serpentinites in the Eastern Desert of Egypt by using Landsat thematic mapper data. Geology 14, 995–999.
Sultan, M., Tucker, R.D., El Alfy, Z., Attia, R., 1994. U-Pb (zircon) ages for the gneissic terrane west of the Nile, southern Egypt. Geol. Rundsch. 83, 514–522.
Surour, A.A., 2016. Chemistry of serpentine "polymorphs" in the Pan-African serpentinites from the Eastern Desert of Egypt, with an emphasis on the effect of superimposed thermal metamorphism. Mineral. Petrol. http://dx.doi.org/10.1007/s00710-016-0460-4 (in press).
Wilde, S.A., Youssef, K., 2000. Significance of SHRIMP U-Pb dating of the imperial porphyry and associated Dokhan volcanics, Gebel Dokhan, north Eastern Desert, Egypt. J. Afr. Earth Sci. 31, 403–413.
Zimmer, M., Kröner, A., Jochum, K.P., Reischmann, T., Todt, W., 1995. The gabal gerf complex: a precambrian N-MORB ophiolite in the Nubian Shield, NE Africa. Chem. Geol. 123, 29–51.
Zoheir, B.A., Lehmann, B., 2010. Listvenite–lode association at the Barramiya gold mine, Eastern Desert, Egypt. Ore Geol. Rev. 39, 101–115.
Zoheir, B.A., El-Shazly, A.K., Helba, H., Khalil, K.I., Bodnar, R.J., 2008. Origin and evolution of the Um Egat and Dungash orogenic gold deposits, Egyptian eastern desert: evidence from fluid inclusions in quartz. Econ. Geol. 103, 405–424.
Zoheir, B.A., Creaser, R.A., Lehman, B., 2014. Re-Os geochronology of gold mineralization in the Fawakhir area, Eastern Desert, Egypt. Int. Geol. Rev. 57, 1418–1432.